AGU PUBLICATIONS

JGR

Journal of Geophysical Research: Atmospheres

RESEARCH ARTICLE
10.1002/2015JD023743

Key Point:
- Aerosol invigoration of cumulus congestus clouds

Correspondence to:
A. M. Sheffield,
asheffie@atmos.colostate.edu

Citation:
Sheffield, A. M., S. M. Saleeby, and S. C. van den Heever (2015), Aerosol-induced mechanisms for cumulus congestus growth, *J. Geophys. Res. Atmos.*, *120*, 8941–8952, doi:10.1002/2015JD023743.

Received 1 JUN 2015
Accepted 11 AUG 2015
Accepted article online 14 AUG 2015
Published online 9 SEP 2015

Aerosol-induced mechanisms for cumulus congestus growth

Amanda M. Sheffield[1], Stephen M. Saleeby[1], and Susan C. van den Heever[1]

[1]Department of Atmospheric Science, Colorado State University, Fort Collins, Colorado, USA

Abstract Tropical convection has been observed to contain three cloud modes, the middle of which is cumulus congestus clouds. Congestus clouds act to moisten the tropical atmosphere, may be mixed-phase, and on occasion surpass the freezing level inversion from where they may develop into deeper convection. This study investigates the impacts of enhanced aerosol concentrations on the growth of congestus clouds produced in idealized cloud-resolving model simulations run under a state of radiative convective equilibrium (RCE). High-resolution, long-duration simulations were completed using the Regional Atmospheric Modeling System (RAMS). Aerosol concentrations between 2 and 4 km above ground level were varied from clean to polluted conditions in order to represent the advection of Saharan dust over the Atlantic Ocean. The congestus populations within each aerosol simulation are statistically analyzed using 10 days of model output after the simulation reaches RCE. Results indicate that congestus in more polluted conditions produce greater amounts of cloud water and ice mass, enhanced updraft strengths, and an increase in the number of congestus cloud tops that extend above the freezing level. Enhanced vapor depositional growth on the populations of more numerous, smaller cloud droplets in the polluted conditions, and the subsequent increase in latent heat release in the warm phase regions of the cloud, is found to be important factors in convective invigoration of these cloud systems. Aerosol feedbacks associated with cold pools and condensate loading also influence the updraft strength and act in opposition to the warm phase invigoration processes.

1. Introduction

The importance of tropical convection in the global water and energy balance has long been recognized [*Riehl and Malkus*, 1958; *Arakawa*, 2004; *Stephens*, 2005]. In the last 15 years or so, the study of the distribution of tropical convection has highlighted the occurrence of tropical cumulus congestus clouds, the middle mode of the trimodal distribution [*Johnson et al*., 1999; *Masunaga et al*., 2005]. The cloud top heights of this tropical mode exist between those of the lower altitude trade wind cumuli and the higher-altitude deep convective clouds. Layers of increased static stability assist in the formation of the trimodal stratification [*Posselt et al*., 2008]. Particular interest exists in congestus as they are important in transporting sensible and latent heat throughout the middle troposphere and plays a fundamental role in the transition from shallow to deep convection [*Johnson and Lin*, 1997; *Johnson et al*., 1999; *Kikuchi and Takayabu*, 2004; *Kuang and Bretherton*, 2006; *Mapes et al*., 2006; *Takayabu et al*., 2010; *Waite and Khouider*, 2010].

Using CloudSat and Moderate Resolution Imaging Spectroradiometer satellite data, *Luo et al*. [2009] found that 30% to 40% of congestus clouds are transient or still developing vertically due to buoyant forcing. The rest of the population was labeled terminal or negatively buoyant. *Jensen and Del Genio* [2006] observed that cumulus congestus clouds contribute to a significant portion of the western Pacific warm pool precipitation. This observation was supported by *Haynes and Stephens* [2007] using CloudSat satellite data, as well as by other previous studies [*Houze and Cheng*, 1977]. Understanding the factors that may control the development of cumulus congestus clouds is thus important to improving our understanding of tropical convection, as well as their representation in convective parameterization schemes [*Kuang and Bretherton*, 2006; *Hohenegger and Stevens*, 2013].

Congestus clouds frequently detrain near cloud top reached in association with the freezing level stable layer, which is typically observed between 4 to 6 km above ground level (agl) in the tropics [*Johnson et al*., 1996; *Takayabu et al*., 2006]. This stable layer has been theorized to form through the melting of ice hydrometeors from dissipating anvils, which generates a cooler layer below the freezing level [*Johnson et al*., 1996, 1999; *Haynes and Stephens*, 2007] and is maintained by a subsidence-induced warmer layer above the freezing level

combined with longwave radiative cooling [*Posselt et al*., 2008]. Previous studies have observed and subsequently defined congestus as having cloud top heights from 3 to 9 km, but this may vary by region [*Johnson et al*., 1999; *Jensen and Del Genio*, 2006]. Several modeling and observational studies have shown the importance of the entrainment of dry air [*Brown and Zhang*, 1997; *Redelsperger et al*., 2002; *Takemi et al*., 2004] in addition to the magnitude of the weak stable layer in determining the depth of congestus.

A further factor potentially influencing the development of tropical convection, including congestus clouds, is the presence of increased aerosol concentrations. The first aerosol indirect effect [*Twomey*, 1974, 1977] and the second aerosol indirect effect or cloud lifetime effect [*Albrecht*, 1989] suggest that for the same liquid water content, an increase in the number of ambient aerosols that are able to serve as cloud condensation nuclei (CCN) results in an increase in cloud droplet number concentrations and a decrease in the average cloud droplet size, thus producing an increase in the cloud albedo and increase in cloud lifetime. Recent work by *Reutter et al*. [2009] examined how an aerosol-limited or updraft-limited cloud can influence cloud droplet nucleation. Aerosol-limited clouds generate high amounts of supersaturation that cannot be used efficiently due to the lack of cloud-nucleating aerosol onto which to condense the excess water vapor. Updraft-limited clouds on the other hand produce low supersaturations and lack the excess water vapor necessary for growth of the aerosol particles present. Conditions between the two extrema are likely to occur.

The updrafts of convective storms appear to be impacted, either directly or indirectly, by the presence of aerosols. Such aerosol-impacted mechanisms include the following: (1) convective invigoration, (2) cold pools, and (3) condensate loading.

1.1. Convective Invigoration

While the aerosol indirect effects discussed above refer to the warm-phase characteristics of cloud droplets and warm rain, once cloud water is lofted above the freezing level it influences the production of ice. In more polluted conditions, an increase in the lofting of cloud water above the freezing level typically occurs as a result of the suppression of the conversion of cloud droplets to raindrops within the warm phase region and reduced precipitation of liquid water. This lofted cloud water is then available to freeze and release latent heat, thereby enhancing the cloud buoyancy and invigorating cloud updrafts [e.g., *Rosenfeld*, 1999, 2000; *Andreae et al*., 2004; *Khain et al*., 2005, 2008; *van den Heever et al*., 2006; *van den Heever and Cotton*, 2007; *Rosenfeld et al*., 2008; *Lee et al*., 2008; *Wang et al*., 2009; *Seigel and van den Heever*, 2012; *Tao et al*., 2012; *Seigel et al*., 2013; *Storer and van den Heever*, 2013]. Although the congestus transition to deep convection is not the focus of this study, a comparison of the relative roles of warm-phase processes compared to the mixed-phase processes in congestus clouds will be examined.

1.2. Cold Pools

Aerosol-induced changes to the cloud droplet size distribution influence the subsequent raindrop size distribution through the collision-coalescence process, thus controlling the evaporation of rain below cloud base. Aerosols have been shown observationally [*Berg et al*., 2008; *May et al*., 2011] and through modeling studies [*Saleeby et al*., 2010, 2015; *Storer et al*., 2010; *Storer and van den Heever*, 2013] to shift the raindrop size distribution to consist of fewer, but larger raindrops, which evaporate less readily in a bulk sense. Reduced evaporation below cloud base due to the presence of increased aerosol concentrations thus results in warmer cold pools. The impacts of aerosol in cold-pool initiated secondary convection in models have been examined [*Khain et al*., 2005; *van den Heever and Cotton*, 2007; *Lee et al*., 2008; *Storer et al*., 2010; *Seigel and van den Heever*, 2012; *Seigel et al*., 2013; *Grant and van den Heever*, 2015; *Saleeby et al*., 2015].

1.3. Condensate Loading

The effects of convective invigoration within deep convective storms are also found to be dependent on the sensitive balance between the buoyancy produced through latent heating and the competing condensate loading effect. In warm phase clouds, *Saleeby et al*. [2015] found that condensate loading typically offsets the latent heating contribution to buoyancy by only 5% when averaged over many cloud lifetimes. *Storer and van den Heever* [2013] found that young, deep convective storm updrafts tend to be controlled predominantly by the release of latent heat, whereas the positive impacts of convective invigoration are more than offset by the negative impacts of aerosol-induced enhanced condensate loading in the mature and dissipating stages.

Complex relationships thus exist between the microphysical and dynamical aspects of aerosol-cloud interactions and motivate this study of the influence of aerosols on cumulus congestus clouds. The research described here is an extension of the cloud resolving modeling study of tropical convection described in *van den Heever et al*. [2011] and *Storer and van den Heever* [2013]. There, the authors investigated the impacts of varying aerosol concentrations on convection produced in large-domain, high-resolution, long-duration simulations conducted under a state of radiative convective equilibrium (RCE). While modeling studies investigating the influence of variations in the environmental thermodynamic profile on congestus growth have been conducted [*Redelsperger et al*., 2002; *Takemi et al*., 2004], few previous studies have specifically focused on aerosol influences on the microphysical properties of congestus with the possible exceptions of *Li et al*. [2013] and *Wall et al*. [2013].

In order to understand the effects of aerosols on all three modes of tropical convection, *van den Heever et al*. [2011] inserted a continuous layer of aerosols that can serve as CCN across the model domain, thus representing the advection of dust within the Saharan Air Layer across the Atlantic Ocean in a highly idealized sense. They found microphysical variations in response to the increased aerosol particle concentrations to be a function of the tropical cloud mode being considered. However, they did not conduct a detailed analysis of the reasons for such cloud type variations. *Storer and van den Heever* [2013] then focused specifically on the impacts of aerosols on deep convective processes.

The goal of the research outlined here is to evaluate the influence of varying aerosol concentrations on the congestus cloud mode within trimodal convection. The large sample of tropical cumulus congestus clouds observed in these RCE simulations allows for a comprehensive and statistically robust study of the microphysical and dynamical responses of these cloud systems to aerosols, and the interactions between these processes. However, the large sample size also makes the tracking of individual storms and their associated processes cumbersome, and hence, impacts as a function of life cycle or individual clouds will not be presented here. Instead, a statistical assessment of aerosol impacts on the congestus population as a whole is conducted. It is found in these simulations that congestus clouds extend above the freezing level more frequently in the more polluted cases. Thus, the focus of this study will be on those aerosol-induced processes that result in the extension of congestus clouds above the freezing level. The relative roles of (1) convective invigoration, (2) cold pool dynamics, and (3) condensate loading will be assessed.

2. Methods

2.1. Model Description

The experiment conducted here is a continuation of the work presented in *van den Heever et al*. [2011] and *Storer and van den Heever* [2013]. The high-resolution cloud-resolving model employed is the Regional Atmospheric Modeling System (RAMS) [*Cotton et al*., 2003]. RAMS is a nonhydrostatic cloud-resolving model (CRM) with advanced microphysics and aerosol schemes [*Walko et al*., 1995; *Meyers et al*., 1997; *Saleeby and Cotton*, 2004; *Saleeby and van den Heever*, 2013]. The RAMS microphysical scheme is a two-moment, bin-emulating bulk scheme that predicts hydrometeor mixing ratio and number concentration for cloud water, rainwater, and five species of ice (pristine ice, snow, aggregates, graupel, and hail). Each is represented by a generalized gamma distribution function. CCN activation is achieved through the use of look-up tables created offline using a parcel model with bin microphysics that considers the saturation ratio, temperature, air and droplet solution density, liquid water content, and air pressure [*Heymsfield and Sabin*, 1989; *Feingold and Heymsfield*, 1992]. Further details on the aerosol parameterization scheme can be found in *Saleeby and Cotton* [2004] and *Saleeby and van den Heever* [2013].

2.2. Model Configuration

The model setup is identical to that used in *Storer and van den Heever* [2013]. While several changes were made to the domain configuration described in *van den Heever et al*. [2011], all of the other model options, as well as the experiment design and approach were the same. The previous study used a two-dimensional grid of 10,000 points at 1 km grid spacing in the zonal direction and 38 vertically stretched points. A two-dimensional grid setup was chosen because of the computational expense of utilizing such a large domain and the long temporal duration necessary to achieve RCE. As discussed in *van den Heever et al*. [2011] and other previous studies [*Tompkins*, 2000; *Stephens et al*., 2008] while the use of two dimensions is expected to influence the broad scales on which the simulated convection organizes, these simulations still capture

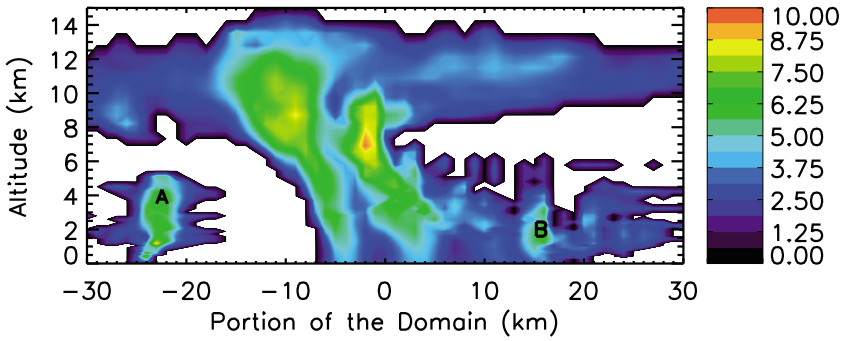

Figure 1. A vertical cross section showing a sample of some of the typical cloud structures in a 60 km subsection of the model domain from the CCN-100 simulations. Shading is total condensate mixing ratio (g kg^{-1}) (contouring begins at 0.5 g kg^{-1}). Two examples of congestus clouds from this study are labeled (*A* and *B*).

many of the fundamental characteristics of tropical convection including the trimodal distribution and the evolution of its middle congestus mode to deep convection and hence much can be learned from them. The model setup used here includes 65 vertically stretched levels reaching ~25 km, which provides greater model resolution of the vertical transport and exchange than in *van den Heever et al*. [2011]. For example, there are 12 levels between the surface and 1 km agl, and the vertical grid spacing near the freezing level is less than 300 m. Horizontal resolution remains at 1 km grid spacing but includes only 7200 points due to computational limitations. Periodic boundary conditions are applied at the lateral boundaries, along with a rigid upper boundary with four Rayleigh absorbing layers to prevent gravity waves from reflecting into the domain and amplifying. A fixed sea surface temperature of 300 K is used. Coriolis force is turned off, and the diurnal cycle has been removed.

The simulations were initialized with a 00:00 UTC 5 December 1992 sounding from the Tropical Ocean–Global Atmosphere Coupled Ocean-Atmosphere Response Experiment [*Webster and Lukas*, 1992], and convection was initiated using randomized perturbations to the low-level potential temperature field. The equilibrated thermodynamic and dynamic structure of the simulated atmosphere evolves from this model setup and includes the development of local- and large-scale circulations. No large-scale forcing is necessary or applied. Radiative convective equilibrium was achieved after ~60 simulation days, similar to that in *van den Heever et al*. [2011], and it was evaluated using the same set of metrics as in that study. As described below, aerosols are added to the model after RCE is reached, and do not significantly alter the state of equilibrium. Additional relevant model options can be found in Table 1 of *van den Heever et al*. [2011].

2.3. Experiment Design

As in *van den Heever et al*. [2011] and *Storer and van den Heever* [2013], aerosol particles that can serve as CCN were inserted in the model between 2 and 4 km agl after RCE was achieved. The aerosol concentrations within the layer were reset each time step, thus representing a constant aerosol source within this layer, similar to what would be observed in a scenario in which dust is continuously advected over a large tropical ocean. The simulations were then allowed to run for an additional 10 days. Even though aerosols are only introduced between 2 and 4 km, they can be advected and diffused throughout the model domain, and hence are found in varying concentrations in the boundary layer, as well as throughout the troposphere. Aerosol activation and nucleation serve as an aerosol sink. The sensitivity tests consist of varying the concentrations of aerosol available to serve as CCN in the 2–4 km agl layer from clean (100 cm^{-3}) to polluted concentrations (200, 400, 800, and 1600 cm^{-3}) and are similar to other previous studies [e.g., *Xue and Feingold*, 2006]. From this point forward, the aerosol sensitivity simulations will be referred to as CCN-100 (100 cm^{-3}), CCN-200 (200 cm^{-3}), CCN-400 (400 cm^{-3}), CCN-800 (800 cm^{-3}), and CCN-1600 (1600 cm^{-3}). Apart from the number of particles available to serve as CCN, the sensitivity setups are otherwise identical. A 60 km sample of the domain containing a convective region from the CCN-100 simulation is shown in Figure 1. This figure demonstrates characteristics similar to previous modeling and observational studies of tropical convection, including a realistic depth of tropical clouds and a trimodal convective cloud distribution [*Johnson et al*., 1999]. Two examples of a congestus cloud are shown in Figure 1 with the labels "A" and "B."

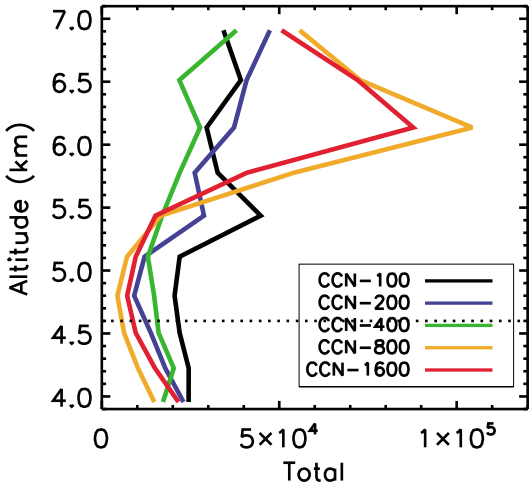

Figure 2. Vertical distribution of cumulus congestus cloud top frequency as a function of aerosol concentration (accumulated from 5 min simulation output over 10 simulation days). Cloud tops were identified by searching from the top of the atmosphere down until a congestus cloud top was found using the congestus criteria. The freezing level is indicated (black dotted line).

2.4. Cumulus Congestus Cloud Selection

Congestus clouds were identified from other forms of convection evident in the simulations based on the following criteria: (1) a continuous cloud column of grid points where the total condensate was greater than 0.01 g kg^{-1}, (2) the cloud base was below 2 km agl, and (3) the cloud top was between 4 and 7 km agl with at least two cloud free vertical grid layers above cloud top (approximately 700–900 m depending on cloud top altitude). The cloud base height requirement was chosen in association with the location of the trade wind inversion at approximately 2 km agl. A maximum cloud top height of 7 km agl was required in order to separate cumulus congestus from the deeper convective mode developing in these simulations. These thresholds were based on observations of congestus from previous studies [*Johnson et al.*, 1999; *Jensen and Del Genio*, 2006; *Haynes and Stephens*, 2007], as well as with what was observed in the model output (Figure 1).

Ten simulation days of data were analyzed at 5 min intervals, thus providing a large sample of congestus clouds from which to construct appropriate statistics. Using the congestus definition described above, up to 350,000 congestus cloud columns were identified over this time period in each simulation. The freezing level is located near 4.5 km agl in these simulations, and hence, the cumulus congestus cloud tops considered here could be above or below the freezing level, as is commonly observed in the tropics.

It is important to note that this study does not distinguish between terminal and transient congestus clouds [*Luo et al.*, 2009], but rather focuses on their microphysical and dynamical characteristics, and the changes induced by varying aerosol concentrations when these cloud tops occur between 4 and 7 km agl. The congestus analyzed here may or may not ultimately continue to grow to deep convection. The very large sample used here allows for a statistically robust investigation of the impacts of aerosols on the mean state of congestus clouds captured in these RCE simulations. Stratification of the aerosol impacts on congestus by environmental characteristics (e.g., vertical wind shear and convective available potential energy) and cloud lifecycle is beyond the scope of this paper but is currently being investigated and will be reported elsewhere.

3. Results

3.1. Cumulus Congestus Cloud Frequency

Figure 2 is a vertical distribution of the 10 day cumulus congestus cloud top frequency (accumulated from 5 min simulation output) as a function of aerosol concentration. This plot was generated by sampling downward from the top of the atmosphere and summing over time the number of cloud tops at each altitude of the congestus cloud columns as identified following the three criteria listed above. The greatest differences are evident between the cleaner cases (CCN-100 and CCN-200) and the more polluted cases (CCN-800 and CCN-1600). Although the increase in cloud top counts is not monotonic, the general trend is one of increasing cloud top frequency with enhanced aerosol concentration. Increasing aerosol concentrations from 100 to 1600 cm^{-3} results in more than double the number of congestus extending to above the freezing level. In addition to increasing the number of congestus, an increased fraction (approximately 5–15%) of congestus clouds are reaching above the freezing level (Table 1) with increased pollution. Enhanced occurrence of congestus clouds above the freezing level appears due to aerosol and the aerosol-cloud interaction causing this increased cloud top frequency will be investigated here.

A corresponding increase in the magnitude of the greatest updraft velocities and the frequency of occurrence at higher altitudes occurs in the more polluted congestus clouds (Figure 3). Figure 3 is a normalized

Table 1. Percentage of Congestus Cloud Tops Identified Below and Above the Freezing Level for the Six Aerosol Simulations

	Freezing Level and Below	Above the Freezing Level
100 cm^{-3}	20.4%	79.6%
200 cm^{-3}	18.7%	81.3%
400 cm^{-3}	21.9%	78.1%
800 cm^{-3}	8.1%	91.9%
1600 cm^{-3}	12.6%	87.4%

contoured frequency by altitude diagram (CFAD) [*Yuter and Houze*, 1995] of updraft speeds (binned by 0.25 m s^{-1}) in congestus clouds from the (a) CCN-100 and (b) CCN-1600 cases. Figure 3c is the difference between the normalized frequencies displayed in Figures 3a and 3b. The normalized frequency in Figures 3a and 3b was calculated by counting the number of occurrences of the range of updraft speeds in each bin at a particular altitude divided by the total number of counts in all updraft speed bins at all altitudes and expressed as a percent. Polluted congestus clouds are found to reach greater maximum updraft speeds and have a shift in the frequency of updrafts to higher altitudes corresponding to deeper cumulus congestus clouds (Figures 2 and 3c).

The increased frequency of congestus clouds above the freezing level in the more polluted cases suggests that various microphysical and/or dynamical changes are occurring as a result of the presence of increased aerosol concentrations. The deeper congestus clouds combined with invigorated updraft speeds have important implications for the development of congestus into deeper convection. The development of deep convection from congestus is beyond this study and we will now focus on those processes that can result in higher congestus cloud tops above the freezing level in more polluted regions.

3.2. Warm Phase Microphysics and Invigoration

Figure 4 shows the vertical profiles of the temporally and spatially averaged total liquid water and total ice water mixing ratios (g kg^{-1}) where updraft velocities are greater than 1 m s^{-1}. This updraft threshold was chosen in order to investigate the microphysical characteristics within the core updraft regions of the congestus clouds systems. It is evident from this figure that the total condensate values are dominated by the liquid water contributions (Figure 4a), which are at least an order of magnitude greater than the average ice mixing ratios (Figure 4b). This indicates that there is relatively little ice mass compared with that of cloud water and rain, even above the freezing level. This is in keeping with the observational studies of *Johnson et al*. [1999]

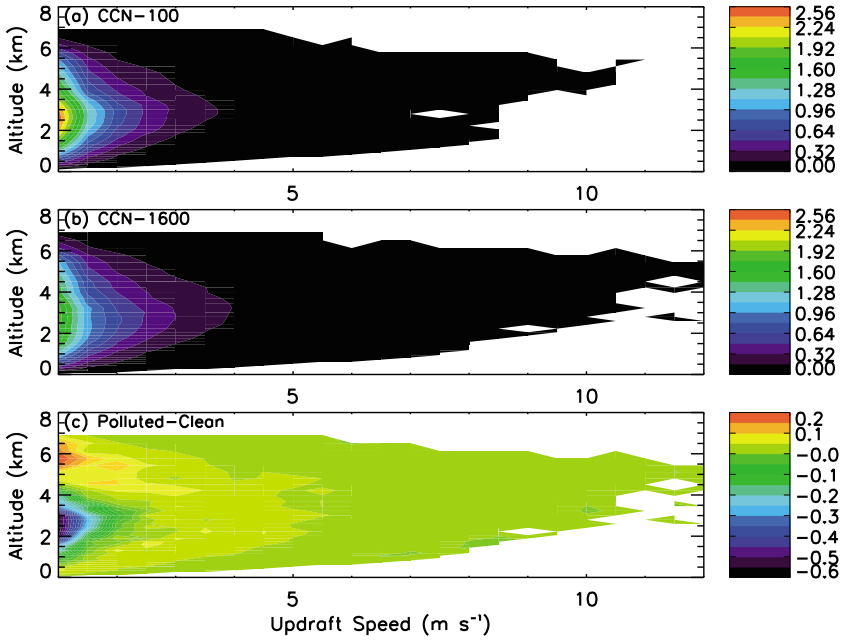

Figure 3. Normalized contoured frequency (%) by altitude diagram (CFAD [*Yuter and Houze*, 1995]) of updraft speeds in cumulus congestus clouds greater than 1 m s^{-1} for aerosol concentrations (cm^{-3}) of (a) 100, (b) 1600, and (c) their difference. The updraft speeds are binned by 0.25 m s^{-1}.

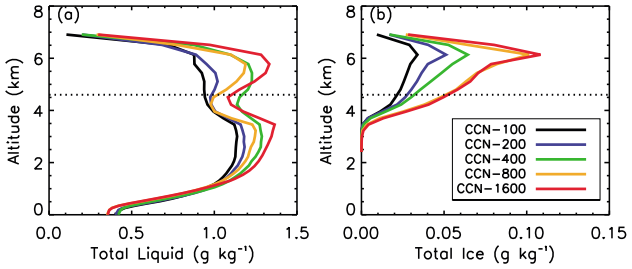

Figure 4. Vertical profiles of the temporally and spatially averaged (a) total liquid water mixing ratio (g kg^{-1}) and (b) total ice mixing ratio (g kg^{-1}) for congestus cloud points where updraft speed is greater than 1 m s^{-1} for varying aerosol concentrations. The dashed line indicates the freezing level. Note that the abscissa scales are different.

and *Zuidema* [1998]. Both the ice and cloud water mass increase in the more polluted clouds, as is noted in previous studies of convective clouds [e.g., *Andreae et al.*, 2004; *van den Heever et al.*, 2006; *Rosenfeld et al.*, 2008].

The contribution of cloud water to the total liquid water mixing ratio tends to be larger than that of rain, except in the lowest levels (Figures 5a and 5d). Figures 5 and 6 are constructed similar to Figure 4 except for the different cloud properties and processes. Cloud water mass is greater in the more polluted scenarios, while the opposite trend is evident for the rainwater. The cloud droplet number concentration is approximately 10 times larger in the most polluted case (CCN-1600) compared to the cleanest case (CCN-100) (Figure 5b), while the average cloud droplet diameters are approximately twice as large in the clean case than in the polluted environments (Figure 5c). Relatively small ice mass occurs in these congestus clouds, but riming and melting do contribute to the trends in the vertical profiles of condensate mass found in Figure 5. Riming of cloud water (Figure 6a) results in the decrease in cloud water content and cloud droplet number concentration evident near the freezing level in Figures 5a and 5b, while the melting of ice (Figure 6b) contributes to the rain mass from approximately 2–4 km agl (Figure 5d). An increase in cloud droplet number concentration above 5 km agl is prominent in the more polluted simulations (Figure 5b), and it is likely due to lofting of cloud droplets from higher updraft speeds (Figure 3) and delayed conversion to precipitation. Only the cleanest and most polluted simulations are shown in Figure 6 for the sake of simplicity.

The response of the rain mass to aerosol loading dominates the total liquid water signal below 1 km agl, producing the weak decreasing trend with enhanced aerosol concentrations in the total liquid water evident in Figure 4a. This result is in keeping with aerosol indirect theory for the warm phase, in that higher concentrations of smaller cloud droplets in the more polluted conditions (Figures 5b and 5c) suppress the collision-coalescence process. Suppression of collision and coalescence results in the reduction in the number concentration of raindrops (Figure 5e); however, the greater abundance of cloud water available for accretion once raindrops do form produces drops that are on average larger in size (Figure 5f). Toward the surface, the average raindrop size was found to increase with proximity to the surface while their number concentration decreased. This trend is due to the full evaporation of smaller drops before larger drops, thus resulting in larger mean raindrop diameters. This change in the raindrop number concentration and size with increased aerosol concentrations has been found in previous modeling studies [*Berg et al.*, 2008; *Saleeby et al.*, 2010; *Storer et al.*, 2010; *Storer and van den Heever*, 2013] and observational studies [*May et al.*, 2011].

The thermodynamic response to the increased aerosol concentration is examined through an analysis of the latent heating budget in association with the predominant microphysical processes. Aerosol-induced changes to the latent heating rates and structure will have an influence on the cloud buoyancy, and hence on the updraft vertical velocities. Processes that contribute to the liquid water mass, and hence changes in the latent heating, include the nucleation of cloud droplets and the growth (demise) by vapor deposition (evaporation) of both cloud droplets and raindrops. Similarly for the ice mass, the nucleation and vapor depositional growth (evaporation) of ice particles and freezing during riming are included. The cleanest and most polluted simulations are again examined here for the sake of simplicity.

The latent heating in association with both liquid water and ice processes increases due to the presence of increased aerosol concentration (Figure 7). Greater aerosol concentration leads to increased cloud droplet number concentration and, thus, cloud droplet surface area. This results in an increased amount of vapor deposition onto cloud droplets, an increase in the conversion from water vapor to liquid, and hence, an increase in the release of latent heat. The enhanced aerosol concentrations are therefore able to more effectively utilize the excess supersaturation generated within the updraft. The comparison of clean and polluted congestus clouds here is similar to the examination of the degree of aerosol limitation described by *Reutter et al.* [2009].

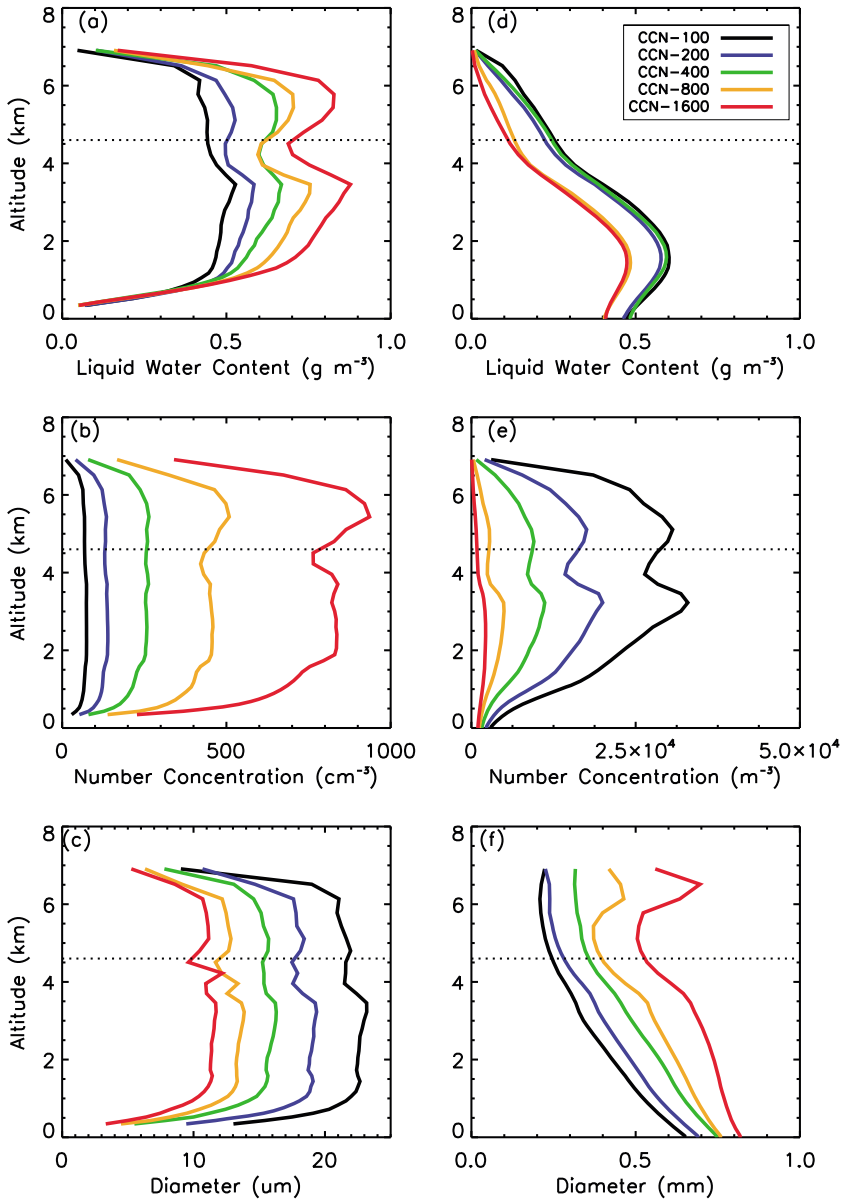

Figure 5. Similar averaging methods as in Figure 4 except for cloud (a) liquid water content (g m^{-3}), (b) droplet number concentration (cm^{-3}), (c) mean droplet diameter (μm), and rain (d) liquid water content (g m^{-3}), (e) drop number concentration (m^{-3}), and (f) mean droplet diameter (mm) for varying aerosol number concentrations (cm^{-3}).

The latent heating from warm phase processes (Figure 7a) is found to be much greater than that released in association with the ice phase processes (Figure 7b). While the ice processes do release latent heat, the relatively small mass of ice produced within these congestus clouds results in relatively minor ice phase contributions to the total in-cloud latent heating. It is apparent from Figure 7 that the warm phase processes, in particular those associated with vapor deposition onto clouds droplets (not shown), dominate the trends in latent heating within the congestus mode.

Warm phase invigoration occurs near and below the freezing level and decreases in magnitude with increasing altitude above the freezing level. Latent heat release in association with the vapor deposition onto ice and freezing during riming begin to become important above the freezing level, but as stated above, their contributions are small compared with that released due to warm phase processes, even above the freezing level. It is important to remember that only congestus clouds are being sampled in this analysis and that this precludes those congestus developing into deep convection from the analysis. While the congestus sampled

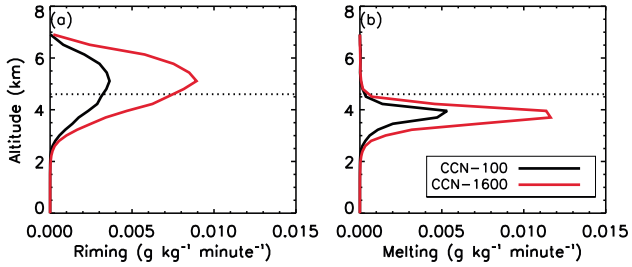

Figure 6. Vertical profiles of the temporally and spatially averaged rate of (a) riming of cloud water (g kg^{-1} min^{-1}) and (b) melting of ice (g kg^{-1} min^{-1}) for congestus cloud points where updraft speed is greater than 1 m s^{-1} for the cleanest and most polluted simulations. The dashed line indicates the freezing level.

here may or may not glaciate and develop into deep convective storms, it is the role of the warm phase invigoration that is emphasized here. Through warm phase invigoration a greater number of congestus clouds with stronger updrafts extend to higher altitudes above the freezing level in the more polluted scenarios. Furthermore, the lifting of more numerous cloud droplets above the freezing level in the polluted cases does enhance the ice phase processes, which could potentially assist with the glaciation and development of these congestus clouds into deep convection. The aerosol-induced warm phase invigoration therefore appears to assist in increasing the availability of congestus above the freezing level for further convective development.

3.3. Cold Pool Dynamics

Several dynamical feedback on the updraft strengths of convective clouds have been suggested in previous studies, including aerosol-induced changes to cold pools [*Berg et al.*, 2008; *Storer et al.*, 2010; *May et al.*, 2011; *Seigel and van den Heever*, 2012; *Seigel et al.*, 2013; *Storer and van den Heever*, 2013; *Saleeby et al.*, 2015]. As shown above, there are fewer raindrops that are larger in size in the more polluted scenarios. Therefore, bulk evaporation rates of the entire raindrop population will be reduced in the more polluted conditions due to the smaller surface area to volume ratio. Thus, polluted congestus are likely to be associated with warmer, and thus weaker cold pools. Similar results were found in association with the deep convective mode in these simulations [*Storer and van den Heever*, 2013]. Given the extremely large database of congestus clouds being considered here, it is difficult to track the cold pool of each congestus clouds individually. However, comparing the temporally and spatially averaged low-level virtual potential temperature perturbation (calculated as the difference between below cloud base and the average clear air region of the domain) for each congestus column, it is evident that the reduced low-level evaporation rates of rain below polluted congestus result in warmer subcloud base temperatures (Figure 8a). It would therefore seem that the weaker, warmer cold pools in the more polluted scenarios are not going to assist in supporting the stronger updrafts and higher cloud tops observed in these cases.

3.4. Condensate Loading

It has been shown above that increased congestus cloud tops and updraft invigoration is occurring in these simulations in association with increased aerosol concentrations. *Storer and van den Heever* [2013] found that in the mature to dissipating stages of the polluted deep convective mode that the negative impacts of aerosol-enhanced condensate loading offset the aerosol-induced latent heating and positive buoyant forcing. Both the magnitude of the buoyancy $\left[g\frac{\theta_v-\theta_o}{\theta_o}\right]$ and the condensate loading [$gr_{condensate}$] in these congestus clouds increases in the more polluted simulations (Figures 8b and 8c, respectively). However, the buoyancy term (Figure 8b) is an order of magnitude larger than the increase in condensate loading occurring in the polluted congestus below the freezing level (Figure 8c). Negative values in the buoyancy profile are due to melting (Figure 6b) and evaporation (Figure 7a) near cloud top. It is apparent from Figure 8 that the increase in condensate loading due to an increase in aerosol is therefore

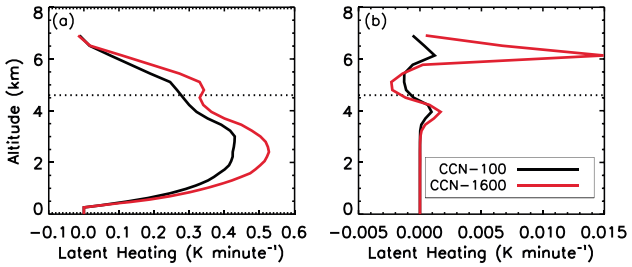

Figure 7. Similar averaging methods as in Figure 6, except for the rate of (a) liquid phase latent heating (K min^{-1}) (nucleation and vapor depositional growth of cloud droplets and raindrops) and (b) ice phase latent heating (K min^{-1}) (nucleation and vapor depositional growth of ice particles, freezing during riming) for the cleanest and most polluted simulations. Note the different scales for the latent heating rates shown.

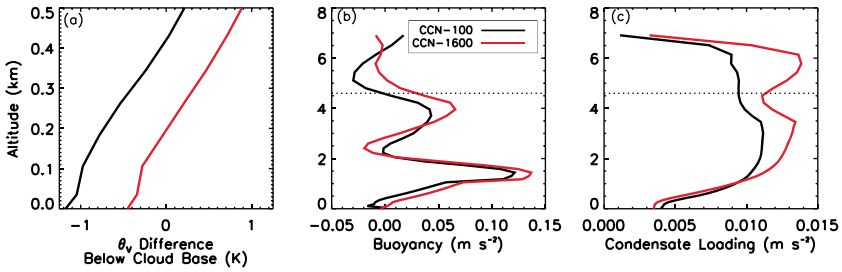

Figure 8. Vertical profiles of temporally and spatially averaged (a) below congestus cloud base virtual potential temperature (θ_v) difference from the clear-sky average θ_o, (b) congestus cloud buoyancy (m s^{-2}) [$g\frac{\theta_v-\theta_o}{\theta_o}$], (c) congestus cloud condensate loading (m s^{-2}) [$gr_{condensate}$]. The dashed line indicates the freezing level. Figures 8b and 8c include averages only where congestus cloud updrafts are greater than 1 m s^{-1} as in Figures 4–7.

less important in this sample of congestus clouds when compared to the mature deep convection within these simulations [*Storer and van den Heever*, 2013]. Similar results were shown recently for shallow cumulus clouds [*Saleeby et al*., 2015]. Therefore, while aerosol impacts on the updrafts of deep convective storms may be positive or negative depending on the stage in the storm lifecycle, aerosol impacts on the updrafts of congestus appear to be predominantly positive.

4. Discussion and Conclusions

This study has investigated the impacts of varying aerosol concentrations on cumulus congestus clouds using high-resolution, long-duration, large-domain RCE simulations. These simulations produced realistic tropical convective systems, with cumulus congestus making up the middle mode of the trimodal tropical cloud distribution. Aerosol-induced microphysical, dynamical, and thermodynamical responses of an extensive sample (up to 350,000 profiles) of congestus clouds have been statistically analyzed.

These simulations demonstrate that the presence of cloud nucleating aerosol enhance the release of latent heat due to warm, liquid phase processes, including cloud droplet nucleation and subsequent vapor depositional growth. In more polluted conditions, this increase is due to the presence of a greater number of smaller clouds droplets and the coincident increase in the total cloud droplet surface area. Increased surface area for vapor deposition hence allows for the more effective utilization of supersaturation generated within the updraft. Even though the ice contents are greater in the more polluted congestus clouds examined here, the actual mass of ice produced is very small in comparison to the liquid water mass. Thus, the contributions of the latent heating to the updraft invigoration in association with ice processes are limited for the congestus population considered here. The aerosol-induced convective invigoration of the updrafts of these congestus clouds therefore occurs primarily in association with the warm phase as opposed to the ice phase. It should be noted that the congestus clouds sampled here have not as yet developed to become deep convection. Should these congestus continue to develop into deep convective towers, it is expected that the ice phase would subsequently play a much more significant role. The important point is that enhanced aerosol concentrations impact congestus clouds through warm phase invigoration, which results in more congestus clouds extending beyond the freezing level more frequently, from where they may remain terminal or alternatively develop into deeper convective systems.

While the warm phase invigoration process appears to be important in enhancing the thermal buoyancy of polluted congestus clouds, previous studies of other cloud types have found that other aerosol-impacted processes, including cold pool lifting and condensate loading [*Storer and van den Heever*, 2013; *Saleeby et al*., 2015; and others], may also impact the strengths of the polluted updrafts. Both cold pool lifting and condensate loading were examined as a function of aerosol loading. Neither of these processes appears to significantly contribute to the increase in congestus cloud top or updraft invigoration.

Finally, as stated above, cumulus congestus are found to occur far more frequently above the freezing level under more polluted conditions. Previous observational studies were inconclusive on the magnitude of this effect due to observational limitations [*Wall et al*., 2013]. A study of the deep convective mode in the same suite of RCE simulations also found increased frequencies of deep convective storms [*Storer and van den Heever*, 2013]. This may be in part due to the enhanced increased frequency of congestus clouds extending

to above the freezing level in the polluted regimes. Aerosol particles may therefore play a potentially important role in the transition of congestus to deep convection by exposing them to mixed phase conditions, additional latent heat release in association with the ice phase, and hence ultimately glaciation. In order to fully unravel the increased frequency of congestus cloud tops above the freezing level in the more polluted cases, the impacts of aerosol-induced microphysical and dynamical processes as a function of congestus life cycle also needs to be examined, as aerosol-driven differences in convective initiation through latent heating may ultimately provide different dynamical and buoyant feedback pathways. These pathways may also be influenced by local environmental characteristics such as vertical wind shear and relative humidity. The impacts of cloud life cycle and the local thermodynamic and dynamical environment on this aerosol response an ongoing area of research by the authors.

In summary, the research presented here has shown that the presence of aerosols may have a significant impact on the growth and properties of cumulus congestus clouds. This impact appears to occur primarily through warm-phase invigoration processes, which lead to stronger updrafts. The presence of enhanced aerosol concentrations results in an increased number of congestus extending above the freezing level inversion, thereby facilitating their potential development to deeper convection upon glaciation. Such a result has significant implications for the moistening of the troposphere, tropical precipitation, and the frequency of deep convection.

Acknowledgments

This research was jointly supported by NASA under grant NNX13AQ33G and by the Department of Energy Office of Science Graduate Fellowship Program, made possible in part by the American Recovery and Reinvestment Act of 2009, administered by ORISE-ORAU under contract DE-AC05-06OR23100. Data can be obtained by contacting A. Sheffield (asheffie@atmos.colostate.edu). The authors would like to thank the two anonymous reviewers of this manuscript for their helpful and constructive suggestions.

References

Albrecht, B. (1989), Aerosols, cloud microphysics, and fractional cloudiness, *Science*, *245*, 1227–1230.

Andreae, M. O., D. Rosenfeld, P. Artaxo, A. A. Costa, G. P. Frank, K. M. Longo, and M. A. F. Silva-Dias (2004), Smoking rain clouds over the amazon, *Science*, *303*, 1337–1342.

Arakawa, A. (2004), The cumulus parameterization problem: Past, present and future, *J. Clim.*, *17*, 2493–2525.

Berg, W., T. L'Ecuyer, and S. C. van den Heever (2008), Evidence for the impact of aerosols on the onset and microphysical properties of rainfall from a combination of satellite observations and cloud-resolving model simulations, *J. Geophys. Res.*, *113*, D14S23, doi:10.1029/2007JD009649.

Brown, R., and C. Zhang (1997), Variability of midtropospheric moisture and its effect on cloud-top height distribution during TOGA COARE, *J. Atmos. Sci.*, *54*, 2760–2774.

Cotton, W. R., et al. (2003), RAMS2001: Current status and future directions, *Meteorol. Atmos. Phys.*, *82*, 5–29.

Feingold, G., and A. J. Heymsfield (1992), Parameterizations of condensational growth of droplets for use in general circulation models, *J. Atmos. Sci.*, *49*, 2325–2342.

Grant, L. D., and S. C. van den Heever (2015), Cold pool responses to aerosol loading: Modulation by dry layers, *J. Atmos. Sci.*, *72*, 1398–1408.

Haynes, J. M., and G. L. Stephens (2007), Tropical oceanic cloudiness and the incidence of precipitation: Early results from CloudSat, *Geophys. Res. Lett.*, *34*, L09811, doi:10.1029/2007GL029335.

Heymsfield, A. J., and R. M. Sabin (1989), Cirrus crystal nucleation by homogeneous freezing of solution droplets, *J. Atmos. Sci.*, *46*, 2252–2264.

Hohenegger, C., and B. Stevens (2013), Preconditioning deep convection with cumulus congestus, *J. Atmos. Sci.*, *70*, 448–464.

Houze, R. A., and C.-P. Cheng (1977), Radar characteristics of tropical convection observed during GATE: Mean properties and trends over the summer season, *Mon. Weather Rev.*, *105*, 964–980.

Jensen, M. P., and A. D. Del Genio (2006), Factors limiting convective cloud-top height at the ARM Nauru Island climate research facility, *J. Clim.*, *19*, 2105–2117.

Johnson, R. H., and X. Lin (1997), Episodic trade wind regimes over the western Pacific warm pool, *J. Atmos. Sci.*, *54*, 2020–2034.

Johnson, R. H., P. E. Ciesielski, and K. A. Hart (1996), Tropical inversions near the 0°C level, *J. Atmos. Sci.*, *53*, 1838–1855.

Johnson, R. H., T. M. Rickenbach, S. A. Rutledge, P. E. Ciesielski, and W. H. Schubert (1999), Trimodal characteristics of tropical convection, *J. Clim.*, *12*, 2397–2418.

Khain, A., D. Rosenfeld, and A. Pokrovsky (2005), Aerosol impact on the dynamics and microphysics of deep convective clouds, *Q. J. R. Meteorol. Soc.*, *131*, 2639–2663.

Khain, A., N. BenMoshe, and A. Pokrovsky (2008), Factors determining the impact of aerosols on surface precipitation from clouds: An attempt at classification, *J. Atmos. Sci.*, *65*, 1721–1748.

Kikuchi, K., and Y. N. Takayabu (2004), The development of organized convection associated with the MJO during TOGA-COARE IOP: Trimodal characteristics, *Geophys. Res. Lett.*, *31*, L10101, doi:10.1029/2004GL019601.

Kuang, Z., and C. S. Bretherton (2006), A mass-flux scheme view of a high-resolution simulation of a transition from shallow to deep cumulus, *J. Atmos. Sci.*, *63*, 1895–1909.

Lee, S. S., L. Donner, and V. Philips (2008), Examination of aerosol effects on precipitation in deep convective clouds during the 1997 ARM summer experiment, *Q. J. R. Meteorol. Soc.*, *134*, 1201–1220.

Li, X., W.-K. Tao, H. Masunaga, G. Gu, and X. Zeng (2013), Aerosol effects on cumulus congestus population over the tropical Pacific: Cloud resolving modeling study, *J. Meteorol. Soc. Jpn.*, *91*, 817–833.

Luo, Z., G. Y. Liu, G. L. Stephens, and R. H. Johnson (2009), Terminal versus transient cumulus congestus: A CloudSat perspective, *Geophys. Res. Lett.*, *36*, L05808, doi:10.1029/2008GL036927.

Mapes, B. E., S. Tulich, J. Lin, and P. Zuidema (2006), The mesoscale convection life cycle: Building blocks or prototypes for large scale tropical waves?, *Dyn. Atmos. Oceans*, *42*, 3–29, doi:10.1016/j.dynatmoce.2006.03.003.

Masunaga, H., T. S. L'Ecuyer, and C. D. Kummerow (2005), Variability in the characteristics of precipitation systems in the tropical Pacific. Part I: Spatial structure, *J. Clim.*, *18*, 823–840.

May, P. T., V. N. Bringi, and M. Thurai (2011), Do we observe aerosol impacts on DSDs in strongly forced tropical thunderstorms?, *J. Atmos. Sci.*, *68*, 1902–1910.

Meyers, M. P., R. L. Walko, J. Y. Harrington, and W. R. Cotton (1997), New RAMS cloud microphysics parameterization. Part II: The two-moment scheme, *Atmos. Res.*, *45*, 3–39.
Posselt, D. J., S. C. van den Heever, and G. L. Stephens (2008), Trimode cloudiness and tropical stable layers at radiative convective equilibrium, *Geophys. Res. Lett.*, *35*, L08802, doi:10.1029/2007GL033029.
Redelsperger, J.-L., D. B. Parsons, and F. Guichard (2002), Recovery processes and factors limiting cloud-top height following the arrival of a dry intrusion observed during TOGA COARE, *J. Atmos. Sci.*, *59*, 2438–2457.
Reutter, P., H. Su, J. Trentmann, M. Simmel, D. Rose, S. S. Gunthe, H. Wernli, M. O. Andreae, and U. Poschl (2009), Aerosol- and updraft-limited regimes of cloud droplet formation: Influence of particle number, size, hygroscopicity on the activation of cloud condensation nuclei (CCN), *Atmos. Chem. Phys.*, *9*, 7067–7080.
Riehl, H., and J. S. Malkus (1958), On the heat balance in the equatorial trough zone, *Geophysica*, *6*, 503–538.
Rosenfeld, D. (1999), TRMM observed first direct evidence of smoke from forest fires inhibiting rainfall, *Geophys. Res. Lett.*, *26*(20), 3105–3108, doi:10.1029/1999GL006066.
Rosenfeld, D. (2000), Suppression of rain and snow by urban and industrial air pollution, *Science*, *287*, 1793–1796.
Rosenfeld, D., U. Lohmann, G. B. Raga, C. D. O'Dowd, M. Kulmala, S. Fuzzi, A. Reissell, and M. O. Andreae (2008), Flood or drought: How do aerosols affect precipitation?, *Science*, *321*, 1309–1313.
Saleeby, S. M., and W. R. Cotton (2004), A large-droplet mode and prognostic number concentration of cloud droplets in the Colorado State University Regional Atmospheric Modeling System (RAMS). Part I: Module descriptions and supercell test simulations, *J. Appl. Meteorol.*, *43*, 182–195.
Saleeby, S. M., and S. C. van den Heever (2013), Developments in the CSU-RAMS aerosol model: Emissions, nucleation, regeneration, deposition, and radiation, *J. Appl. Meteorol. Climatol.*, *52*, 2601–2622.
Saleeby, S. M., W. Berg, S. C. van den Heever, and T. L'Ecuyer (2010), Impact of cloud-nucleating aerosols in cloud-resolving model simulations of warm-rain precipitation in the East China Sea, *J. Atmos. Sci.*, *67*, 3916–3930.
Saleeby, S. M., S. R. Herbener, S. C. van den Heever, and T. L'Ecuyer (2015), Impacts of cloud droplet nucleating aerosols on shallow tropical convection, *J. Atmos. Sci.*, *72*, 1398–1408.
Seigel, R. B., and S. C. van den Heever (2012), Dust lofting and ingestion by supercells, *J. Atmos. Sci.*, *69*, 1453–1473.
Seigel, R. B., S. C. van den Heever, and S. M. Saleeby (2013), Mineral dust indirect effects and cloud radiative feedbacks of a simulated idealized nocturnal squall line, *Atmos. Chem. Phys.*, *13*, 4467–4485.
Stephens, G. L. (2005), Cloud feedback in the climate system: A critical review, *J. Clim.*, *18*, 237–273.
Stephens, G. L., S. C. van den Heever, and L. A. Pakula (2008), Radiative-convective feedbacks in idealized states of radiative-convective equilibrium, *J. Atmos. Sci.*, *65*, 3899–3916.
Storer, R. L., and S. C. van den Heever (2013), Microphysical processes evident in aerosol forcing of tropical deep convection, *J. Atmos. Sci.*, *70*, 430–446.
Storer, R. L., S. C. van den Heever, and G. L. Stephens (2010), Modeling aerosol impacts on convective storms in different environments, *J. Atmos. Sci.*, *67*, 3904–3915.
Takayabu, Y. N., J. Yokomori, and K. Yoneyama (2006), A diagnostic study on interactions between atmospheric thermodynamic structure and cumulus convection over the tropical western Pacific Ocean and over the Indochina peninsula, *J. Metoerol. Soc. Jpn.*, *84*, 151–169.
Takayabu, Y. N., S. Shige, W.-K. Tao, and N. Hirota (2010), Shallow and deep latent heating modes over tropical oceans observed with TRMM spectral latent heating data, *J. Clim.*, *23*, 2030–2046.
Takemi, T., O. Hirayama, and C. Liu (2004), Factors responsible for the vertical development of tropical oceanic cumulus convection, *Geophys. Res. Lett.*, *31*, L11109, doi:10.1029/2004GL020225.
Tao, W.-K., J.-P. Chen, Z. Li, C. Wang, and C. Zhang (2012), Impact of aerosols on convective clouds and precipitation, *Rev. Geophys.*, *50*, RG2001, doi:10.1029/2011RG000369.
Tompkins, A. M. (2000), The impact of dimensionality on long-term cloud-resolving model simulations, *Mon. Weather Rev.*, *128*, 1521–1535.
Twomey, S. (1974), Pollution and the planetary albedo, *Atmos. Environ.*, *8*, 1251–1256.
Twomey, S. (1977), The influence of pollution on the short wave albedo of clouds, *J. Atmos. Sci.*, *34*, 1149–1152.
van den Heever, S. C., and W. R. Cotton (2007), Urban aerosol impacts on downwind convective storms, *J. Appl. Meteorol. Climatol.*, *46*, 828–850.
van den Heever, S. C., G. G. Carrio, W. R. Cotton, P. J. DeMott, and A. J. Prenni (2006), Impacts of nucleating aerosol on Florida storms. Part I: Mesoscale simulations, *J. Atmos. Sci.*, *63*, 1752–1775.
van den Heever, S. C., G. L. Stephens, and N. B. Wood (2011), Aerosol indirect effects on tropical convection characteristics under conditions of radiative-convective equilibrium, *J. Atmos. Sci.*, *68*, 699–718.
Waite, M. L., and B. Khouider (2010), The deepening of tropical convection by congestus preconditioning, *J. Atmos. Sci.*, *67*, 2601–2615.
Walko, R. L., W. R. Cotton, M. P. Meyers, and J. Y. Harrington (1995), New RAMS cloud microphysics parameterization. Part I: The single-moment scheme, *Atmos. Res.*, *38*, 29–62.
Wall, C., C. Liu, and E. Zipser (2013), A climatology of tropical congestus using CloudSat, *J. Geophys. Res. Atmos.*, *118*, 6478–6492, doi:10.1002/jgrd.50455.
Wang, J., S. C. van den Heever, and J. S. Reid (2009), A conceptual model for the link between Central American biomass burning aerosols and severe weather over south central United States, *Environ. Res. Lett.*, *4*, 015003, doi:10.1088/1748-9326/4/1/015003.
Webster, P. J., and R. Lukas (1992), TOGA COARE: The Coupled Ocean–Atmosphere Response Experiment, *Bull. Am. Meteorol. Soc.*, *73*, 1377–1416.
Xue, H., and G. Feingold (2006), Large-eddy simulations of trade win cumuli: Investigation of aerosol indirect effects, *J. Atmos. Sci.*, *63*, 1605–1622.
Yuter, S. E., and R. A. Houze Jr. (1995), Three dimensional kinematic and microphysical evolution of Florida cumulonimbus. Part II: Frequency distributions of vertical velocity, reflectivity and differential reflectivity, *Mon. Weather Rev.*, *123*, 1941–1963.
Zuidema, P. (1998), On the 600–800 mb minimum in tropical cloudiness, *J. Atmos. Sci.*, *55*, 2220–2228.